3-2015

Investigation of Electromagnetic Velocities and Negative Refraction in a Chiral Metamaterial with Second-order Material Dispersion using Spectral Analyses and Dispersive Models

Monish Ranjan Chatterjee
University of Dayton, mchatterjee1@udayton.edu

Tarig A. Algadey
University of Dayton

Optical Engineering

OpticalEngineering.SPIEDigitalLibrary.org

Investigation of electromagnetic velocities and negative refraction in a chiral metamaterial with second-order material dispersion using spectral analyses and dispersive models

Monish R. Chatterjee
Tarig A. Algadey

SPIE.

Investigation of electromagnetic velocities and negative refraction in a chiral metamaterial with second-order material dispersion using spectral analyses and dispersive models

Monish R. Chatterjee* **and Tarig A. Algadey**
University of Dayton, Department of Electrical and Computer Engineering, 300 College Park, Dayton, Ohio 45469, United States

Abstract. In recent years, considerable research has been carried out relative to the electromagnetic (EM) propagation and refraction characteristics in metamaterials with emphasis on the origins of negative refractive index. Negative refractive index may be introduced in metamaterials via different methods; one such is the condition whereby the Poynting vector of the EM wave is in opposition to the group velocity in the material. Alternatively, negative refractive index also occurs when the group and phase velocities in the medium are in opposition. The latter phenomenon has been extensively investigated in the literature, including recent work involving chiral metamaterials with material dispersion up to the first order. This paper examines the possible emergence of negative refractive index in dispersive chiral metamaterials with material dispersion up to the second order. The motivation is to determine if using second- as opposed to first-order dispersion may lead to more practical negative index behavior. A spectral approach combined with a slowly time-varying phasor analysis is applied, leading to the analytic derivation of EM phase and group velocities, and the resulting phase and group velocities and the corresponding phase and group indices are evaluated by selecting somewhat arbitrary dispersive parameters. The results indicate the emergence of negative index (via negative phase indices along with positive group indices, as reported in the literature) or negative index material (NIM) behavior over information bandwidths in the low RF range. The second-order results are not significantly better than those for first-order results based on the theoretical analysis; however, greater parametric flexibility exists for the second-order system leading to the higher likelihood of achieving NIM over practical frequency bands. The velocities and indices computed using the Lorentzian and Condon models yield an NIM bandwidth around 200 – 400 Mrad/ sec, about 2 orders of magnitude higher than that for the parametric approach; more importantly, NIM is found not to occur in the first order when using practical models. [DOI: 10.1117/1.OE.54.3.037108]

Keywords: phase velocity; energy velocity; group velocity; circular polarization; higher order dispersion; Poynting vector; chiral constitutive relations; chirality; negative index; contra-propagation; material dispersion.

Paper 150073P received Jan. 16, 2015; accepted for publication Mar. 6, 2015; published online Mar. 24, 2015.

1 Introduction

It is known that counter propagation between such standard electromagnetic (EM) entities as the Poynting vector, the propagation vector, the group velocity and the phase velocity (in paired combinations) leads to the onset of negative refractive index behavior in the material.[1–6] Over the past 15 or more years, several research studies have focused on the emergence of, and consequent behavior due to negative index in such (meta)materials corresponding to several different domains of operation and their potential applications.[7–9] Since refractive index in a material is typically expressed via the phase and group indices, it is natural to determine which of these (perhaps one or both) would become negative in the negative index material (NIM) regime. It has been shown that in the NIM regime, the group index (n_g) remains positive, while it is the phase index (n_p) which becomes negative.[10] In Valanju et al.,[10] these properties are verified both experimentally and via simulations. Dong et al.[11] have reported that in the NIM regime, both the medium permittivity and permeability are negative (as is well known), and the corresponding EM behavior (whereupon the phase velocity inside the metamaterial is negative) is described as left handed. It is commonly found that NIM behavior is more readily realizable at microwave frequencies, and in particular in some composites.[8,12] Realizing NIM at optical frequencies continues to be more challenging, particularly because samples tend to be thin and exhibit high degrees of dissipation.[13] Since under counter propagation of phase and group velocities in a metamaterial (one of the prerequisites for NIM behavior) both the permeability and permittivity assume negative values, it turns out that the phase index in such a situation is to be regarded as the negative root of the product of the relative permeability and permittivity; similarly, with both permeability and permittivity being negative, a real phase velocity emerges with a negative sign. This real velocity ensures EM propagation in the medium; however, since the regime is NIM, the group velocity (and consequently the group index) is positive here. Since n_p is negative in NIM, the resulting effects for

*Address all correspondence to: Monish R. Chatterjee, E-mail: mchatterjee1@udayton.edu

0091-3286 /2015/$25.00 © 2015 SPIE

refraction under Snell's law are very different than customarily happens in ordinary (positive) index materials. One consequence is that at the NIM interface, one generates a backward wave for which the phase moves in a direction opposite to the direction of the energy flow.[14] It has already been noted that achieving a negative index in the optical frequency range is much more complicated for several reasons. However, it turns out that the permittivities of a variety of materials (especially metals) tend to be very large at RF or microwave frequencies, and are dramatically reduced in the optical band. Hence, nominally, NIM is difficult to achieve at optical frequencies. Fortunately, it also turns out that at optical frequencies the EM response of metals is vastly different from those at lower (RF or microwave) frequencies, where the permittivity is extremely large and metals behave as nearly perfect conductors. At optical frequencies, the permittivity of metals may become comparable to the dielectric permittivity of a host material, allowing the excitation of a surface plasmon resonance that leads to another means of achieving negative permittivity and permeability, thereby allowing negative index behavior at optical frequencies.[15]

In recent work, Banerjee and Chatterjee investigated the EM propagational velocities in a chiral metamaterial under material dispersion due to dispersive permittivity, permeability and chirality up to the first order (assuming a lossless material).[1] The analysis involved applying relevant constitutive relations to Maxwell's equations combined with slowly time-varying phasors and Fourier transforms, thereby developing plane wave solutions for the electric and magnetic fields. This approach led to the usual finding of three possible wavenumbers of propagation as functions of frequency and the different material parameters. Using one of these wavenumbers, it was possible to derive the phase, group, and energy velocities for these plane waves by assuming first-order dispersion in each of the three parameters in terms of the modulation/sideband frequency. The operational/carrier frequency could be in any chosen band, including RF or optical. Normalizing the velocities and applying practical dispersive models led to frequency-dependent phase and group indices, and it was shown that the material may operate in the negative index (NIM) region within arbitrary (modulation) frequency bands.[1] Overall, this first-order analysis demonstrated that that NIM behavior occurs under counter-propagation of either the Poynting vector and the propagation vector, or alternatively the phase and group velocities. The first-order analysis indicated that opposition of phase and group velocities could be achieved over certain sideband frequency windows for specific choices of first-order dispersive parameters. Furthermore, by assuming standard dispersive models, it was possible to predict the velocity counter-propagation windows and the corresponding negative index windows by adapting the models to the spectral analysis carried out for EM propagation in a dispersive chiral material. A primary motivation for conducting the second-order analysis presented in this work is to incorporate dispersive effects that may be tailored up to the second order in each of the primary parameters (permittivity, permeability, and chirality) used in the spectral analysis. Since the NIM windows in a sideband frequency are determined by the choices of the dispersive parameters, it is reasonable to assume that one would have greater flexibility in achieving desired NIM bands and negative index amplitudes when working up to the second order. In reality, as we show later, a set of first- and second-order parameters actually produces a wider NIM window in the first-order compared to the second order. However, such an occurrence is only due to the specific choice of parameters examined in this analysis. Obviously, for other choices of the parameters, one may expect widening of the NIM band in the second order. Adaptation of the dispersive models to the second-order problem likewise yields practical and probably realizable values of both the negative indices and the NIM bands. Upon further examination, it is found that NIM behavior using the model-based analyses occurs only under second-order dispersion. When examined under first-order with chosen practical parameter values compatible with those used for the second order, it is shown that NIM does not occur. Furthermore, it is found that while the physical values of the indices tend to be impractical under the assumed theoretical/parametric models, the corresponding values found under model-based analyses are actually quite compatible with that seen in the literature (thus, the negative phase index ranges in the neighborhood of typically -1 to -5). Finally, the absence of NIM under first-order model-based analyses indicates a significant difference from the corresponding second-order result, highlighting the importance of second-order analysis as pursued in this paper.

In Sec. 2, we present a quick review of EM field solutions under first-order material dispersion and associated propagation velocities previously derived by Banerjee and Chatterjee.[1] We then examine the effect on the field components and velocities when dispersion via material parameters is considered up to the second order, i.e., up to order $O(\Omega^2)$ in sideband frequency, as will be explained in Sec. 3 in some detail. We show that once again the fields exhibit circular polarization, a property that manifests itself in chiral materials independent of the order of dispersion.[6] It is shown that the derived results are consistent with the cases of zeroth- and first-order dispersions. Additionally, we find that in order to reduce the dispersive material problem to the non-chiral limit, one cannot simply set the chirality parameter to zero and expect the usual results to follow. The coupling effect of chirality-induced constitutive relations obviously induces fundamental changes in the physical equations governing EM propagation. The motivation for analysis up to the second order arises from not only the desire to find the differences that occur under group-velocity-type dispersion (which typically occurs in second order), but also to see if additional parametric flexibilities might exist in terms of achieving negative index behavior in the material in realizable frequency ranges and numerical magnitudes of the physical quantities involved. As will be shown, such flexibilities likely emerge under the assumptions made, and to emphasize the more novel features of this analysis, a section in the text is devoted to direct comparisons between the first- and second-order computations. Incidentally, normalized expressions for the energy velocity ($\tilde{v}_{e3}$) based on the Poynting vector and the stored energy density inside the medium have been derived and certain interesting conditions observed that specifically enable the velocity to be written in an amplitude-independent form. Energy velocity derivations, however, will not be discussed in this paper. Normalized phase and group velocities ($\tilde{v}_{p3N}$ and $\tilde{v}_{g3N}$)

are obtained after considerable algebra in Sec. 3, and it turns out that these are obtainable without the parametric balances that become necessary when deriving the energy velocity. It is evident from these results that the resulting dependence on Ω is much more extensive than in the first-order case.[6] Direct comparisons for phase and group velocities, sideband resonances, negative index domains, and actual realized phase and group indices are also carried out in Sec. 4 in some detail. Section 5 concludes this paper with a summary of the derived second-order fields, velocities, and indices and their similarities and differences with respect to the standard dispersionless and first-order results.

2 Brief Overview of Electromagnetic EM Analysis Under First-Order Dispersion

The negative index in the presence of chirality and material dispersion up to the first order has been studied by Banerjee and Chatterjee.[1] The basic methodology consists of using Maxwell's equations, constitutive relations, spectral analyses, and plane wave solutions to eventually obtain the group, phase, and energy velocities in the medium, and thereafter finding conditions for the negative index.[16] A typical schematic scenario leading to negative index is shown in Fig. 1. Starting with expansions of the material parameters up to the first order, one may express the frequency-dependent chirality parameter, electric permittivity, and the magnetic permeability in first-order Taylor expansions. Next, the EM constitutive relations for a reciprocal chiral medium in the frequency domain are incorporated into the standard Maxwell's curl equations. Using Fourier transforms and the constitutive relations, a set of nontrivial plane-wave field solutions are derived, from where four possible solutions for the wavenumber in the medium compatible with the plane wave under investigation are obtained.[17] Using the wavenumber $\tilde{k}_{z3}$ (for illustration purposes) given by

$$\tilde{k}_{z3} = -\omega\tilde{\kappa}_P\sqrt{\mu_0\varepsilon_0} + \omega\sqrt{\tilde{\mu}_p\tilde{\varepsilon}_p}, \tag{1}$$

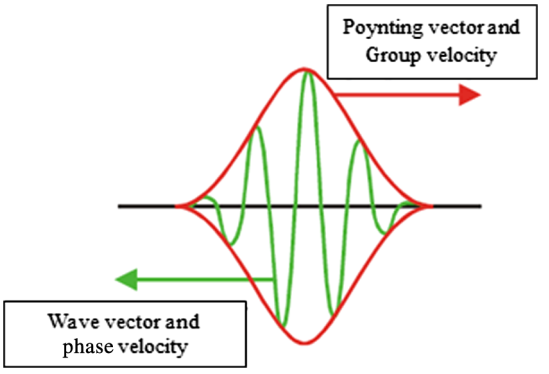

Fig. 1 Conditions leading to possible onset of negative index behavior (after Ref. 16).

the field solutions are obtained in terms of a "free" amplitude $\tilde{E}_{px}$ as[1]

$$\tilde{E}_{px}, \text{arbitrary}, \tag{2}$$

$$\tilde{E}_{py} = \frac{-\omega^2\tilde{\mu}_p\tilde{\varepsilon}_p + \tilde{\alpha}_p^2 + \tilde{k}_z^2}{2j\tilde{\alpha}_p\tilde{k}_z}\tilde{E}_{px}, \tag{3}$$

$$\tilde{H}_{px} = \frac{-\tilde{k}_z^2 + \omega^2\tilde{\mu}_p\tilde{\varepsilon}_p + \tilde{\alpha}_p^2}{2j\tilde{\alpha}_p\omega\tilde{\mu}_p}\tilde{E}_{px}, \tag{4}$$

$$\tilde{H}_{py} = \frac{-\tilde{\alpha}_p^2 + \tilde{k}_z^2 + \omega^2\tilde{\mu}_p\tilde{\varepsilon}_p}{2\omega\tilde{\mu}_p\tilde{k}_z}\tilde{E}_{px}. \tag{5}$$

By using the second relation (3), it is shown that in the presence of chirality the electric field is indeed circularly polarized $\tilde{E}_{py} = j\tilde{E}_{px}$, as is the magnetic field.

To find the phase and group velocities, defining $\tilde{v}_p(\Omega) = 1/(k_z/\omega)$ and $\tilde{v}_g(\Omega) = 1/(\partial k_{z3}/\partial\Omega) = 1/(\partial k_{z3}/\partial\omega)$, one finally obtains the velocities as follows:[1]

$$\tilde{v}_{p3}(\Omega) = \frac{1}{\left\{\left(-\tilde{\kappa}_{p0}\sqrt{\mu_0\varepsilon_0} + \sqrt{\tilde{\mu}_{p0}\tilde{\varepsilon}_{p0}}\right) + \Omega\left[\frac{1}{2}\frac{(\tilde{\varepsilon}_{p0}\tilde{\mu}'_{p0}+\tilde{\varepsilon}'_{p0}\tilde{\mu}_{p0})\sqrt{\tilde{\mu}_{p0}\tilde{\varepsilon}_{p0}}}{\tilde{\mu}_{p0}\tilde{\varepsilon}_{p0}} - \sqrt{\mu_0\varepsilon_0}\tilde{\kappa}'_{p0}\right]\right\}}\hat{a}_z, \tag{6}$$

and

$$\tilde{v}_{g3}(\Omega) = \frac{1}{\left\{\begin{array}{c}\left[-\tilde{\kappa}_{p0}\sqrt{\mu_0\varepsilon_0} - \omega_0\tilde{\kappa}'_{p0}\sqrt{\mu_0\varepsilon_0}\right.\\ \left.+\sqrt{\tilde{\mu}_{p0}\tilde{\varepsilon}_{p0}}\frac{\omega_0}{2}\frac{(\tilde{\varepsilon}_{p0}\tilde{\mu}'_{p0}+\tilde{\varepsilon}'_{p0}\tilde{\mu}_{p0})}{\tilde{\mu}_{p0}\tilde{\varepsilon}_{p0}} + \sqrt{\tilde{\mu}_{p0}\tilde{\varepsilon}_{p0}}\right]\\ +\Omega\left[-2\tilde{\kappa}'_{p0}\sqrt{\mu_0\varepsilon_0} + \sqrt{\tilde{\mu}_{p0}\tilde{\varepsilon}_{p0}}\frac{(\tilde{\varepsilon}_{p0}\tilde{\mu}'_{p0}+\tilde{\varepsilon}'_{p0}\tilde{\mu}_{p0})}{\tilde{\mu}_{p0}\tilde{\varepsilon}_{p0}}\right.\\ \left.+\frac{\sqrt{\tilde{\mu}_{p0}\tilde{\varepsilon}_{p0}}}{2}\frac{(\omega_0)(2\tilde{\varepsilon}'_{p0}\tilde{\mu}'_{p0}+\tilde{\varepsilon}_{p0}+\tilde{\mu}_{p0})}{\tilde{\mu}_{p0}\tilde{\varepsilon}_{p0}}\right.\\ \left.-\frac{1}{4}\sqrt{\tilde{\mu}_{p0}\tilde{\varepsilon}_{p0}}\frac{(\omega_0)(\tilde{\varepsilon}_{p0}\tilde{\mu}'_{p0}+\tilde{\varepsilon}'_{p0}\tilde{\mu}_{p0})^2}{\tilde{\mu}_{p0}^2\tilde{\varepsilon}_{p0}^2}\right]\end{array}\right\}}\hat{a}_z. \tag{7}$$

3 Spectral Analysis Leading to Negative Index Under Second-Order Dispersion

In this section, we begin by expanding the material parameters as defined earlier up to the second order in frequency using the Taylor series, so that

$$\begin{bmatrix}\tilde{\varepsilon}_p(\Omega)\\ \tilde{\mu}_p(\Omega)\\ \tilde{\alpha}_p(\Omega)\end{bmatrix} = \begin{bmatrix}\tilde{\varepsilon}_{p0}(\Omega) + (\Omega)\tilde{\varepsilon}'_{p0} + (\Omega^2/2)\tilde{\varepsilon}''_{p0}\\ \tilde{\mu}_{p0}(\Omega) + (\Omega)\tilde{\mu}'_{p0} + (\Omega^2/2)\tilde{\mu}''_{p0}\\ \omega\sqrt{\mu_0\varepsilon_0}(\tilde{\kappa}_{p0} + (\Omega)\tilde{\kappa}'_{p0} + (\Omega^2/2)\tilde{\kappa}''_{p0})\end{bmatrix}. \tag{8}$$

We next express $\tilde{k}_{z3}$ in terms of the chiral wave number $\tilde{\alpha}_p$ as

$$\tilde{k}_{z3}^2 = (-\tilde{\alpha}_p + \omega\sqrt{\tilde{\mu}_p\tilde{\varepsilon}_p})^2 = \tilde{\alpha}_p^2 - 2\omega\tilde{\alpha}_p\sqrt{\tilde{\mu}_p\tilde{\varepsilon}_p} + \omega^2\tilde{\mu}_p\tilde{\varepsilon}_p. \tag{9}$$

Substituting the various frequency-dependent terms into Eq. (3), and after considerable algebra,[1] we may express the field components to the second order in terms of parametric coefficients as follows:

$$\tilde{E}_{px}(\Omega), \text{arbitrary} \tag{10}$$

$$\tilde{E}_{py}(\Omega) = j(A_{13} + \Omega B_{13} + \Omega^2 C_{13})\tilde{E}_{px}(\Omega), \tag{11}$$

$$\tilde{H}_{px}(\Omega) = j(A_{23} + \Omega B_{23} + \Omega^2 C_{23})\tilde{E}_{px}(\Omega), \tag{12}$$

$$\tilde{H}_{py}(\Omega) = j(A_{33} + \Omega B_{33} + \Omega^2 C_{33})\tilde{E}_{px}(\Omega). \tag{13}$$

Carrying out the necessary algebra, first these coefficients are found to be

$$A_{13} = 1, \quad B_{13} = 0, \quad C_{13} = 0. \tag{14}$$

Substituting the above in Eq. (11) immediately indicates that once again $\tilde{E}_{py} = j\tilde{E}_{px}$. This result implies that even under second-order dispersion, the EM field in the presence of chirality usually exhibits circular polarization, as was also seen in the first-order case.[1] Thus, the presence of the chiral constitutive relations in the EM analysis automatically leads to circular polarization, independent of dispersion. The resulting Y-component of the electric field leads the X-component by 90 deg.

Substituting $\tilde{k}_{z3}$ and $\tilde{\alpha}_p$ into Eq. (4), the magnetic field component $\tilde{H}_{px}$ may be written as

$$\tilde{H}_{px} = -j\frac{\sqrt{\tilde{\varepsilon}_p}}{\sqrt{\tilde{\mu}_p}}\tilde{E}_{px}, \tag{15}$$

where, using Eqs. (8) and (12), the corresponding coefficients are found to be

$$A_{23} = -\sqrt{\frac{\tilde{\varepsilon}_{p0}}{\tilde{\mu}_{p0}}}, \tag{16}$$

$$B_{23} = -\sqrt{\frac{\tilde{\varepsilon}_{p0}}{\tilde{\mu}_{p0}}}\left(\frac{\tilde{\varepsilon}'_{po}}{2\tilde{\varepsilon}_{p0}} - \frac{\tilde{\mu}'_{po}}{2\tilde{\mu}_{p0}}\right), \tag{17}$$

and

$$C_{23} = -\sqrt{\frac{\tilde{\varepsilon}_{p0}}{\tilde{\mu}_{p0}}}\left(\frac{1}{4}\frac{\tilde{\varepsilon}''_{po}}{\tilde{\varepsilon}_{p0}} - \frac{1}{8}\frac{\tilde{\varepsilon}'^2_{po}}{\tilde{\varepsilon}^2_{p0}} - \frac{\tilde{\mu}'_{po}}{2\tilde{\mu}_{p0}}\frac{\tilde{\varepsilon}'_{po}}{2\tilde{\varepsilon}_{p0}} - \frac{1}{4}\frac{\tilde{\mu}''_{po}}{\tilde{\mu}_{p0}} + \frac{3}{8}\frac{\tilde{\mu}'^2_{po}}{\tilde{\mu}^2_{p0}}\right). \tag{18}$$

Finally, using Eqs. (8) and (13), we obtain the last series of coefficients as

$$A_{33} = -A_{23} = \sqrt{\frac{\tilde{\varepsilon}_{p0}}{\tilde{\mu}_{p0}}}, \tag{19}$$

$$B_{33} = -B_{23} = \sqrt{\frac{\tilde{\varepsilon}_{p0}}{\tilde{\mu}_{p0}}}\left(\frac{\tilde{\varepsilon}'_{po}}{2\tilde{\varepsilon}_{p0}} - \frac{\tilde{\mu}'_{po}}{2\tilde{\mu}_{p0}}\right), \tag{20}$$

and

$$C_{33} = -C_{23} = \sqrt{\frac{\tilde{\varepsilon}_{p0}}{\tilde{\mu}_{p0}}}\left(\frac{1}{4}\frac{\tilde{\varepsilon}''_{po}}{\tilde{\varepsilon}_{p0}} - \frac{1}{8}\frac{\tilde{\varepsilon}'^2_{po}}{\tilde{\varepsilon}^2_{p0}} - \frac{\tilde{\mu}'_{po}}{2\tilde{\mu}_{p0}}\frac{\tilde{\varepsilon}'_{po}}{2\tilde{\varepsilon}_{p0}} - \frac{1}{4}\frac{\tilde{\mu}''_{po}}{\tilde{\mu}_{p0}} + \frac{3}{8}\frac{\tilde{\mu}'^2_{po}}{\tilde{\mu}^2_{p0}}\right). \tag{21}$$

Once again, consistent with chiral behavior, we find that $\tilde{H}_{py} = j\tilde{H}_{px}$, indicating circular polarization. In what follows, we primarily use the frequency dependence of the wavenumber to find the phase and group velocities under dispersion. For these calculations, field amplitude information is not needed. However, if calculating the energy velocity ($\tilde{v}_e$), the field amplitudes are necessary in order to compute the Poynting vector and the stored energy. In the present work, energy velocity is not pursued.

3.1 *Derivation of Phase Velocity from Spectral Analysis*

Using the relation $\tilde{v}_p(\Omega) = 1/(k_{z3}/\omega)$, we may calculate the phase velocity by using $\tilde{k}_{z3}$ and retaining up to the second order in Ω, as described below. Hence, beginning with

$$\tilde{v}_{p3}(\Omega) = \frac{1}{\left(-\tilde{\kappa}_p\sqrt{\mu_0\varepsilon_0} + \sqrt{\tilde{\mu}_p\tilde{\varepsilon}_p}\right)}, \tag{22}$$

and using appropriate expansions, we finally get

$$\tilde{v}_{p3}(\Omega) = \frac{1}{\left\{\begin{array}{c}\left[-\tilde{\kappa}_{p0}\sqrt{\mu_0\varepsilon_0} + \left(\sqrt{\tilde{\mu}_{p0}\tilde{\varepsilon}_{p0}}\right)\right] \\ +\Omega\left[\frac{1}{2}\frac{(\tilde{\varepsilon}_{p0}\tilde{\mu}'_{p0}+\tilde{\varepsilon}'_{p0}\tilde{\mu}_{p0})\sqrt{\tilde{\mu}_{p0}\tilde{\varepsilon}_{p0}}}{\tilde{\mu}_{p0}\tilde{\varepsilon}_{p0}} - \sqrt{\mu_0\varepsilon_0}\tilde{\kappa}'_{p0}\right] \\ +\Omega^2\left[-\frac{1}{2}\sqrt{\mu_0\varepsilon_0}\tilde{\kappa}''_{p0} + \frac{1}{4}\frac{(2\tilde{\varepsilon}'_{p0}\tilde{\mu}'_{p0}+\tilde{\varepsilon}_{p0}\tilde{\mu}''_{p0}+\tilde{\varepsilon}''_{p0}\tilde{\mu}_{p0})\sqrt{\tilde{\mu}_{p0}\tilde{\varepsilon}_{p0}}}{\tilde{\mu}_{p0}\tilde{\varepsilon}_{p0}}\right. \\ \left. -\frac{1}{8}\frac{(\tilde{\varepsilon}_{p0}\tilde{\mu}'_{p0}+\tilde{\varepsilon}'_{p0}\tilde{\mu}_{p0})^2\sqrt{\tilde{\mu}_{p0}\tilde{\varepsilon}_{p0}}}{\tilde{\mu}^2_{p0}\tilde{\varepsilon}^2_{p0}}\right]\end{array}\right\}}, \tag{23}$$

It turns out that by applying the parametric ratio condition, ratios $\tilde{\varepsilon}'_{po}/\tilde{\varepsilon}_{p0} = \tilde{\mu}'_{po}/\tilde{\mu}_{p0}$ and $\tilde{\varepsilon}''_{po}/\tilde{\varepsilon}_{p0} = \tilde{\mu}''_{po}/\tilde{\mu}_{p0}$, the phase velocity in Eq. (22) simplifies to

$$\tilde{v}_{p3}(\Omega) = \frac{(1/\sqrt{\mu_0\varepsilon_0})}{\left\{\begin{array}{c}\left(-\tilde{\kappa}_{p0} + \sqrt{\tilde{\varepsilon}_r\tilde{\mu}_r}\right) + \Omega\left[\left(\frac{\tilde{\varepsilon}'_{po}}{\tilde{\varepsilon}_{p0}}\right)\sqrt{\tilde{\varepsilon}_r\tilde{\mu}_r} - \tilde{\kappa}'_{p0}\right] \\ +\Omega^2\left(-\frac{1}{2}\tilde{\kappa}''_{p0} + \frac{2}{4}\sqrt{\tilde{\varepsilon}_r\tilde{\mu}_r}\frac{\tilde{\varepsilon}''_{po}}{\tilde{\varepsilon}_{p0}}\right)\end{array}\right\}}. \tag{24}$$

We note that the condition stated above is not necessary for evaluating the velocity; it merely makes the algebra slightly simpler. Also, the result in Eq. (24) reverts to the first-order case upon eliminating the second-order terms.[1]

3.2 *Derivation of Group Velocity from Spectral Analysis*

We next calculate group velocity using the definition,

$$\tilde{v}_g(\Omega) = \frac{1}{(\partial k_{z3}/\partial\Omega)} = \frac{1}{(\partial k_{z3}/\partial\omega)}. \tag{25}$$

Applying the same parametric ratio condition as for the phase velocity, we rewrite the group velocity in a relatively simplified form as follows:

$$\begin{aligned}\tilde{v}_{g3}(\Omega) = {} & \frac{(1/\sqrt{\mu_0\varepsilon_0})}{\left\{\left[-\tilde{\kappa}_{p0} - \omega_0\tilde{\kappa}'_{p0} + \sqrt{\tilde{\varepsilon}_r\tilde{\mu}_r}\frac{\omega_0}{2}\left(2\frac{\tilde{\varepsilon}'_{p0}}{\tilde{\varepsilon}_{p0}}\right) + \sqrt{\tilde{\varepsilon}_r\tilde{\mu}_r}\right]\right\}} \\ & + \left\{\Omega\left[(-2)\tilde{\kappa}'_{p0} - \omega_0\tilde{\kappa}''_{p0} + \sqrt{\tilde{\varepsilon}_r\tilde{\mu}_r}\left(2\frac{\tilde{\varepsilon}'_{p0}}{\tilde{\varepsilon}_{p0}}\right)\right.\right. \\ & \left.\left. + \sqrt{\tilde{\varepsilon}_r\tilde{\mu}_r}\omega_0\left(\frac{\tilde{\varepsilon}'^2_{po}}{\tilde{\varepsilon}^2_{po}} + \frac{\tilde{\varepsilon}''_{po}}{\tilde{\varepsilon}_{po}}\right) - \sqrt{\tilde{\varepsilon}_r\tilde{\mu}_r}\omega_0\left(\frac{\tilde{\varepsilon}'^2_{po}}{\tilde{\varepsilon}^2_{po}}\right)\right]\right\} \\ & + \left\{\Omega^2\left[\left(-\frac{3}{2}\right)\tilde{\kappa}''_{p0} + \frac{3}{2}\left(\frac{\tilde{\varepsilon}'^2_{po}}{\tilde{\varepsilon}^2_{po}} + \frac{\tilde{\varepsilon}''_{po}}{\tilde{\varepsilon}_{po}}\right)\sqrt{\tilde{\varepsilon}_r\tilde{\mu}_r}\right.\right. \\ & \left.\left. - \frac{3}{2}\sqrt{\tilde{\varepsilon}_r\tilde{\mu}_r}\left(\frac{\tilde{\varepsilon}'^2_{po}}{\tilde{\varepsilon}^2_{po}}\right)\right]\right\}. \end{aligned} \tag{26}$$

Note that the group velocity depends on Ω, Ω^2 (sideband frequency) and ω_0 (carrier frequency). As with $\tilde{v}_{p3}(\Omega)$, the result in Eq. (26) reverts to the first order upon eliminating all second-order terms.[1]

4 Numerical Results and Interpretations

In the following, we present numerical results for the phase and group velocities pertinent to first- and second-order dispersions upon making certain simplifying parametric assumptions. We first examine the frequency-dependent (normalized) phase velocity. This is followed by similar graphical examination of the (normalized) group velocity. The plots are carried out for both first- and second-order dispersions for comparison purposes. The velocity plots are followed by plots of the phase and group refractive indices, again under first- and second-order approximations. In each case, it is found that there exists a region or band within which the velocities are in opposition (the so-called negative index material or NIM region). Fortuitously, we also find that it is the phase index which is negative in the NIM region, while the group index remains positive. Likewise, the phase velocity in the NIM region is negative, while the group velocity is positive. These results are found to be consistently true in the analyses presented here, and are in agreement with known results in the literature.[5,7,8,10] The overall results are then compared and the trends in first- and second-order analyses are assessed.

4.1 *Phase Velocity and Phase Index Under First- and Second-Order Dispersions*

We examine the frequency behavior of the phase velocity normalized relative to the free-space value of c. The plot of $\tilde{v}_{p3N}(\Omega)$ versus frequency is carried out by assuming $\tilde{\mu}_r = \tilde{\varepsilon}_r = 4$, $\tilde{\kappa}_{p0} = 5$. Rewriting Eq. (24) as follows:

$$\tilde{v}_{p3N}(\Omega) = \frac{1}{\left\{-1 + \Omega\left[\left(\frac{\tilde{\varepsilon}'_{po}}{\varepsilon_0}\right) - \tilde{\kappa}'_{p0}\right] + \Omega^2\left(-\frac{1}{2}\tilde{\kappa}''_{p0} + \frac{\tilde{\varepsilon}''_{po}}{2\varepsilon_0}\right)\right\}},$$

or equivalently

$$\tilde{v}_{p3N}(\Omega) = \frac{1}{c + b\Omega + a\Omega^2}, \text{ in the second order} \tag{27}$$

and

$$\tilde{v}_{p3N}(\Omega) = \frac{1}{c + b\Omega}, \text{ in the first order} \tag{28}$$

where a, b, and c are the parameter-dependent constants derived from Eq. (27).

4.1.1 *Phase velocity under first-order dispersion*

We choose $\tilde{\kappa}'_{p0} = 0.1(\tilde{\varepsilon}'_{po}/\varepsilon_0)$ and $\tilde{\varepsilon}'_{po} = 3.13\times10^{-18}$ in order to place the velocity resonance or transition in the neighborhood of a sideband around a few Mrad/sec. With the chosen values, the phase velocity transitions under first-order material dispersion around (Ω_t) approximately 3.17×10^6 rad/sec. If $\Omega < \Omega_t$, denominator <0, then $\tilde{v}_{p3N}(\Omega) < 0$. On the other hand, if $\Omega > \Omega_t$, and denominator >0, then $\tilde{v}_{p3N}(\Omega) > 0$. Figure 2(a) shows the phase velocity over the frequency interval $0 \le \Omega < 2\pi f_{\max}$, where $f_{\max} = 10^6$ Hz. From the plot we can see that the transition frequency is around 3.17×10^6 rad/sec. This reasonably matches the numerical value. We note that in this instance, $\tilde{v}_p$ transitions from negative to positive around Ω_t. Figure 2(b) shows the phase index n_{p3} which is calculated by using $n_{p3} \triangleq 1/v_{p3N}$ and drawn over the interval $0 \le \Omega < 2\pi f_{\max}$. The phase index plot shows that n_{p3} passes through zero and the transition frequency Ω_t, and becomes negative for $\Omega < \Omega_t$ and positive for $\Omega > \Omega_t$. Thus, the NIM region exists in the range $0 \le \Omega \le \Omega_t$. We also observe that the numerical value of n_{p3} ranges approximately from 1.2 to –1 in the NIM. These numbers matched up well with practical values seen in the theocratical and experimental literature.[8,10,11]

4.1.2 *Phase velocity under second-order dispersion*

Using Eq. (28) with the appropriate coefficients and parameters, the normalized phase velocity is plotted and the results are shown in Fig. 2(c). For this case, we additionally choose $\tilde{\kappa}''_{p0} = 0.1(\tilde{\varepsilon}''_{po}/\varepsilon_0)$ and $\tilde{\varepsilon}''_{p0} = 0.25\times10^{-24}$. We note that these parameters along with those for the first order are again selected in order to produce sideband resonances around a few Mrad/sec. From the plot we note that the (positive) resonant frequency Ω_r is around 2.72×10^6 rad/sec. We see that in this instance, $\tilde{v}_{p3}$ again transitions from negative to positive around the resonance.

Proceeding as in the first-order case, we define the phase index $n_{p3} \triangleq 1/v_{p3N} = c + b\Omega + a\Omega^2$, and obtain the phase index shown in Fig. 2(d).

As before, n_{p3} transitions from zero around the resonance to negative below Ω_r and positive above. Therefore, the NIM is expected in the range $0 \le \Omega \le \Omega_r$. The physical range of n_{p3} values in second order are 1.6 to –1, in fair agreement with the literature.[10,13]

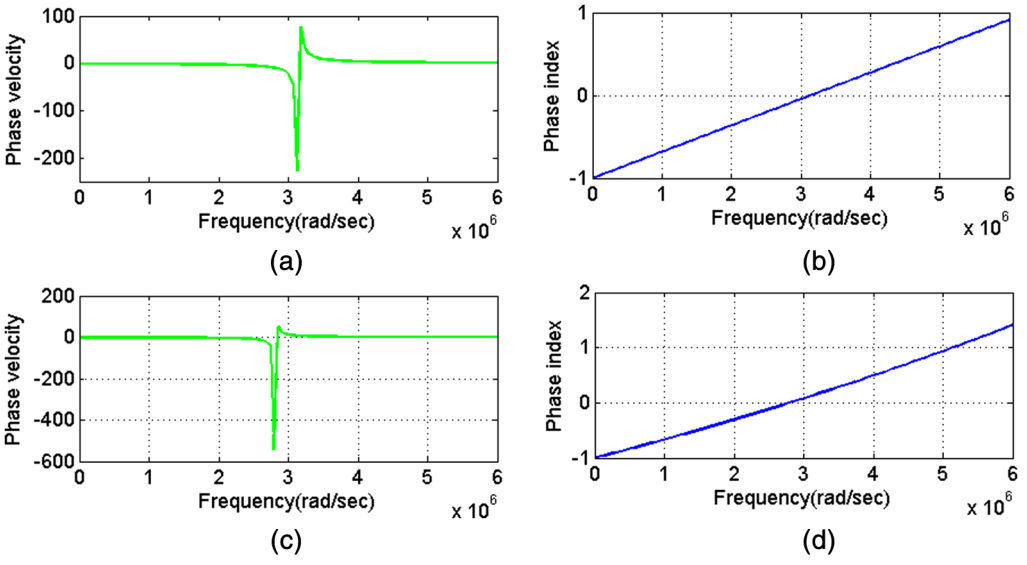

Fig. 2 Phase velocity and phase index (a) $\tilde{v}_{p3}$ under first order; (b) n_{p3} under first order; (c) $\tilde{v}_{p3}$ under second order; (d) n_{p3} under second order.

4.2 *Group Velocity and Group Index Under First- and Second-Order Dispersions*

To determine and plot the (normalized) group velocity dispersion, we substitute again the material parameters $\tilde{\mu}_r = \tilde{\varepsilon}_r = 4$, $\tilde{\kappa}_{p0} = 5$, and $\tilde{\varepsilon}_{p0} = \varepsilon_r\varepsilon_0$ in Eq. (26). This leads to

$$\tilde{v}_{g3N}(\Omega) = \frac{1}{(a + b\Omega + c\Omega^2)}, \tag{29}$$

with parametric-dependent constants $a = -1 - \omega_0\tilde{\kappa}'_{p0} + \omega_0(\tilde{\varepsilon}'_{p0}/\varepsilon_0)$, $b = -2\tilde{\kappa}'_{p0} - \omega_0\tilde{\kappa}''_{p0} + \omega_0(\tilde{\varepsilon}''_{p0}/\varepsilon_0) + 2(\tilde{\varepsilon}'_{p0}/\varepsilon_0)$, $c = -(3/2)\tilde{\kappa}''_{p0} + (3/2)(\tilde{\varepsilon}''_{p0}/\varepsilon_0)$, $\omega_0 = 10^{14}$ rad/ sec. We observe here that in the plots that follow, some of the chosen parameters (such as the carrier ω_0) are selected in accordance with values used in the literature.[6]

4.2.1 *Group velocity under first-order dispersion*

For the first order, we chose $\tilde{\kappa}'_{p0} = 0.1(\tilde{\varepsilon}'_{po}/\varepsilon_0)$, and again $\tilde{\varepsilon}'_{po} = 3.13 \times 10^{-18}$, as were chosen for phase velocity. Also, note that the transition frequency is now negative (around approximately -5.24×10^{13} rad/ sec). The group velocity transitions from negative to positive for frequencies higher than -5.24×10^{13} rad/ sec. For $\Omega > 0$, we observe that $\tilde{v}_{g3}$ is consistently positive. A last observation regarding the physical values of $\tilde{v}_{p3N}$ and $\tilde{v}_{g3N}$ is in order here. For the parametric chosen, $\tilde{v}_{p3N}$ tends to be up to 2 orders of magnitude higher than c, while $\tilde{v}_{g3N}$ is up to 6 orders of magnitude above c. These somewhat unexpected values, however, are still compatible with other numerical findings[7,12,14] as in Fig. 3(a).

The group index calculated by using $n_{g3} \triangleq 1/v_{g3N}$ is shown in Fig. 3(b). We observe that n_{g3} once again passes

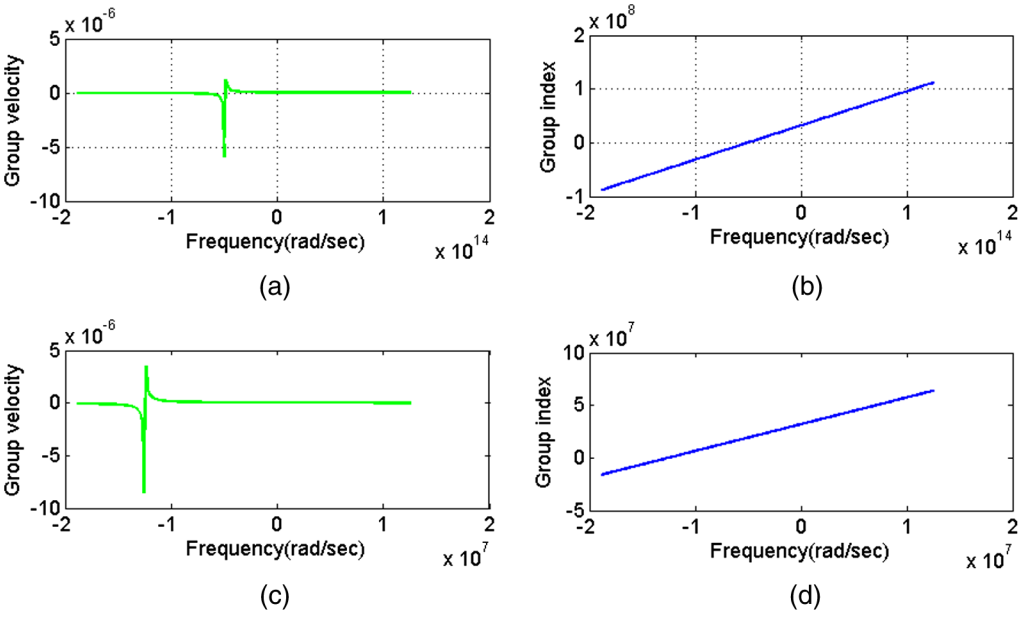

Fig. 3 Group velocity and group index (a) $\tilde{v}_{p3}$ under first order; (b) n_{p3} under first order; (c) $\tilde{v}_{p3}$ under second order; (d) n_{p3} under second order.

through zero around the (negative) transition frequency Ω_t, and is negative for $\Omega < \Omega_t$ and positive for $\Omega > \Omega_t$. Since $\Omega_t < 0$, the negative group index behavior is irrelevant to the NIM band (which must fall within a positive frequency band). This shall be discussed further later. Also to be noted is the fact that the numerical value of n_{g3} varies from about 0.6×10^8 to -0.6×10^8. Both these are exceptionally high, but are a consequence of the unusually low values of v_{g3N} derived earlier.

4.2.2 *Group velocity under second-order dispersion*

Under second-order dispersion, first-and second-order parameters are again selected identical to those used for phase velocity. Using the appropriate parameter, the plot shown in Fig. 3(c) is obtained. It turns out that for the chosen parameters, both resonances of $\tilde{v}_{g3N}$ are negative, of which the less negative is shown in Fig. 3(c). Once again, the group velocity transitions from negative to positive around the resonance frequency (about -1.26×10^7 rad/ sec). The nature of $\tilde{v}_{g3N}$ at $\Omega > 0$ is again consistently positive. Figure 3(d) shows the group index under second-order dispersion with the chosen parameters. As in the first-order case, the group index once again transitions from negative to positive around the resonance. Since the NIM region discussed later falls in the positive frequency band, $\tilde{n}_{g3}$ will be consistently positive within the NIM band. This result is in agreement with the literature.[10] The numerical values of $\tilde{n}_{g3N}$ in the second order are again unusually large, as expected.

4.3 *Note on Direct Comparison between $\tilde{n}_{p3}$ and $\tilde{n}_{g3}$*

For the purpose of comparing the phase and group velocities for a given set of material constants across a range of frequencies, we next illustrate the cases represented by Figs. 2(a) and 3(a). We note from Fig. 2(a) that for the specific choice of material constants, the phase velocity transitions from negative to positive around the resonance. Likewise, the group velocity also transitions from negative to positive around the resonance as seen from Fig. 3(a). These transitions are further indicated in the index plots of Figs. 2(b) and 3(b). In Fig. 4, which schematically graphs the signs of both indices under the first order together, we find that the indices n_{p3} and n_{g3} are in opposition within the frequency range of approximately -5.24×10^{-13} rad/ sec up to about 3.17 Mrad/ sec. Hence, it is expected that the material may exhibit negative index characteristics in this range. In practice, of course, the proper NIM region exists for positive frequencies only; this "usable" band is shown in Fig. 4 from 0 to Ω_{tp}. A similar schematic band picture of n_{p3} and n_{g3} is shown in Fig. 5 for second-order dispersion. The usable NIM in this case turns out to be slightly narrower. However, this is of no great significance, as will be discussed later. Overall, it is established from those analyses that n_{p3} is always negative and n_{g3} is always positive in the NIM, as expected.[10]

5 Application of Practical Dispersive Models to the Second-Order System

To study the performance of the chiral dispersive materials in terms of the normalized phase and group velocities derived previously for propagating signals consisting of pulsed or modulated carriers, we take up the Lorentzian dispersive models for relative permittivity and permeability and the Condon model for chirality, as follows:[1,6]

$$\tilde{\varepsilon}_{pr}(\omega) = 1 + \frac{(\omega_p^2)}{(\omega_c^2 - \omega^2)}, \tag{30}$$

$$\tilde{\mu}_{pr}(\omega) = 1 + \frac{(\omega_m^2)}{(\omega_c^2 - \omega^2)}, \tag{31}$$

$$\tilde{\kappa}_{pr}(\omega) = \alpha_c \frac{(\omega)}{(\omega_c^2 - \omega^2)}, \tag{32}$$

where $\tilde{\varepsilon}_{pr}(\omega)$, $\tilde{\mu}_{pr}(\omega)$, and $\tilde{\kappa}_{pr}(\omega)$ are respectively the relative (spectral) permittivity, permeability, and chirality admittance of the material under consideration. The frequencies ω_p and ω_m arise from electric polarization and magnetization, respectively, while ω_c represents a (single) resonance in the neighborhood of the applied signal. Also α_c represents a chiral frequency parameter. From Eq. (23), we have the

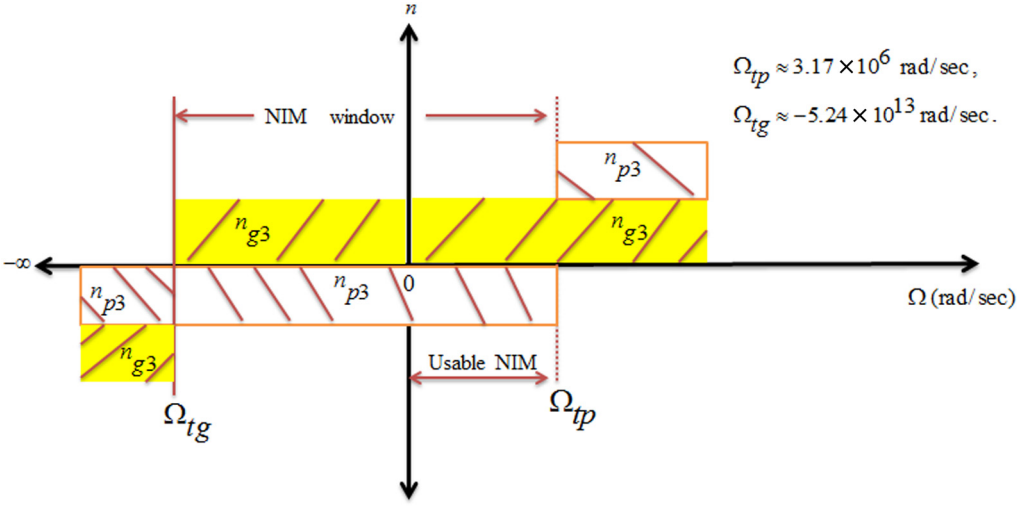

Fig. 4 Index distribution showing the (positive) frequency band (NIM region) where n_{p3} and n_{g3} are in opposition under first-order material dispersion.

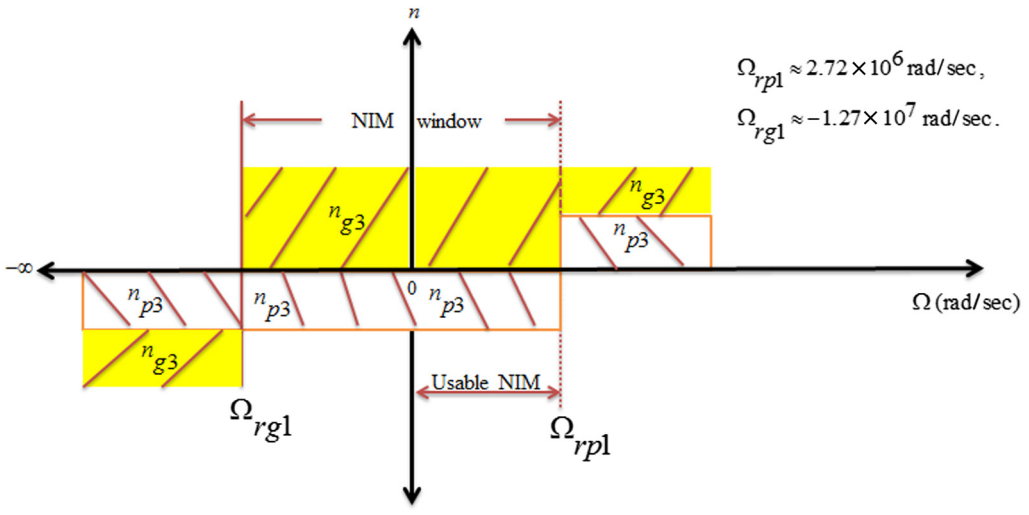

Fig. 5 Index distribution showing the (positive) frequency band (NIM region) where n_{p3} and n_{g3} are in opposition under second-order material dispersion.

relativity permittivity under second-order material dispersion as follows:

$$\tilde{\varepsilon}_p(\Omega) = \tilde{\varepsilon}_{p0} + (\Omega)\tilde{\varepsilon}'_{p0} + (\Omega^2/2)\tilde{\varepsilon}''_{p0}, \tag{33}$$

where the sideband frequency Ω is equal to $\Omega = \omega - \omega_0$, and ω_0 is the carrier frequency. We may note that typically $\Omega \ll \omega_0$, therefore, while the carrier may be in the optical domain, the sideband may well be in the RF (thus in the MHz-GHz range).

In the case of $\Omega \ll \omega_c$, the relative spectral permittivity in Eq. (30) can be written as follows:

$$\tilde{\varepsilon}_{pr}(\omega) = 1 + \frac{\frac{\omega_p^2}{\omega_c^2}}{\left(1 - \frac{\omega^2}{\omega_c^2}\right)}. \tag{34}$$

Using Taylor expansion up to the second order for the equation above and assuming $\Omega \ll \omega_c$ and $\omega_0 \ll \omega_c$, and comparing Eq. (30) with Eq. (33), we will have the following:

$$\tilde{\varepsilon}'_{pr0} = \frac{\tilde{\varepsilon}'_{p0}}{\tilde{\varepsilon}_{p0}} = \frac{2\omega_0\omega_p^2}{\omega_c^4}, \tag{35}$$

$$\tilde{\varepsilon}''_{pr0} = \frac{\tilde{\varepsilon}''_{p0}}{2\tilde{\varepsilon}_{p0}} = \frac{\omega_p^2}{\omega_c^4}, \tag{36}$$

$$\tilde{\varepsilon}_{pr0} = 1 + \frac{\omega_p^2}{\omega_c^2}, \tag{37}$$

Similarly, from the relative (spectral) permeability relation and comparing with the Lorentzian dispersive model for relative permeability in Eq. (31), we get the following:

$$\frac{\tilde{\mu}_p(\Omega)}{\tilde{\mu}_{p0}(\Omega)} = 1 + \frac{\Omega\tilde{\mu}'_{p0}}{\tilde{\mu}_{p0}} + \frac{(\Omega^2/2)}{\tilde{\mu}_{p0}}\tilde{\mu}''_{p0}, \tag{38}$$

$$\tilde{\mu}'_{pr0} = \frac{\tilde{\mu}'_{p0}}{\tilde{\mu}_{p0}} = \frac{2\omega_0\omega_m^2}{\omega_c^4}, \tag{39}$$

$$\tilde{\mu}''_{pr0} = \frac{\tilde{\mu}''_{p0}}{2\tilde{\mu}_{p0}} = \frac{\omega_m^2}{\omega_c^4}, \tag{40}$$

$$\tilde{\mu}_{pr0} = 1 + \frac{\omega_m^2}{\omega_c^2}, \tag{41}$$

Finally, based on the chirality expression up to second-order material dispersion, the chiral coefficients may be derived as follows:

$$\tilde{\kappa}_p(\Omega) = \tilde{\kappa}_{p0} + (\Omega)\tilde{\kappa}'_{p0} + (\Omega^2/2)\tilde{\kappa}''_{p0}. \tag{42}$$

Upon then applying the Condon model as in Eq. (32), we obtain the following:

$$\tilde{\kappa}_{pr0} = \alpha_c\frac{\omega_0}{\omega_c^2}, \tag{43}$$

$$\tilde{\kappa}'_{pr0} = \frac{\tilde{\kappa}'_{p0}}{\tilde{\kappa}_{p0}} = \alpha_c\frac{1}{\omega_c^2}, \tag{44}$$

$$\tilde{\kappa}''_{pr0} = \frac{\tilde{\kappa}''_{p0}}{\tilde{\kappa}_{p0}} = 6\alpha_c\frac{\omega_0}{\omega_c^4}. \tag{45}$$

We next substitute Eqs. (35) to (37), (23) to (41), and (43) to (45) into Eq. (27) to compute the normalized phase velocity under the Lorentzian dispersive model for relative permittivity and permeability and the Condon model for chirality. After considerable algebra, we obtain the (normalized) phase velocity as in Eq. (34).[6] To plot phase velocity versus the sideband frequency we assume plausible values for ω_p, ω_m and ω_c[18,19] Thus, we begin with the phase velocity as above in Eq. (28)

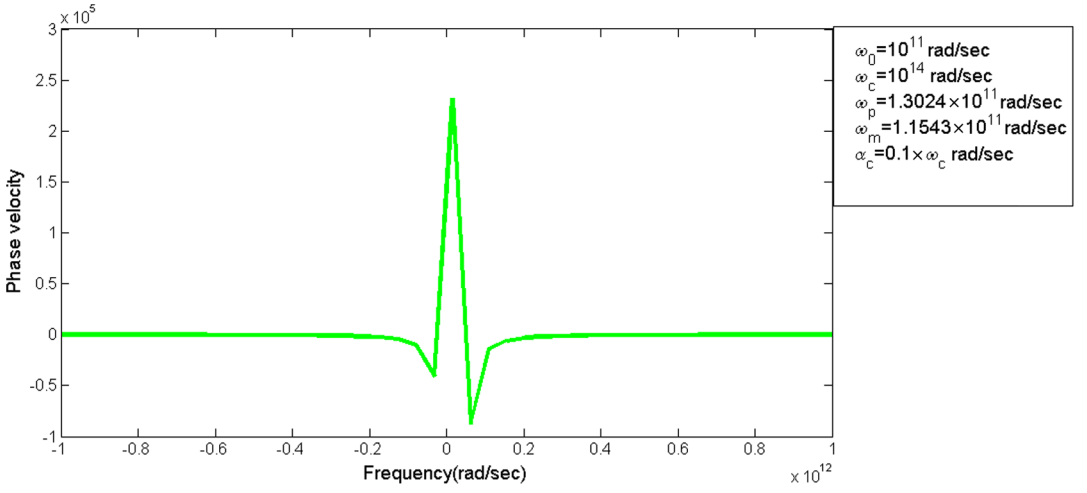

Fig. 6 The modeled phase velocity under second order.

$$\tilde{v}_{p3N}(\Omega) = \frac{1}{\left\{-1+\Omega\left[\left(\frac{8\omega_0\omega_p^2}{\omega_c^4}\right)-\alpha_c\frac{\tilde{\kappa}_{p0}}{\omega_c^2}\right]+\Omega^2\left(-15\alpha_c\frac{\omega_0}{\omega_c^4}+\frac{8\omega_p^2}{\omega_c^4}\right)\right\}}. \quad (46)$$

The (positive) phase velocity resonance is at approximately 6.28×10^{10} rad/sec. From the plot in Fig. 6 we note that in this instance, $\tilde{v}_{p3N}$ transitions from negative to positive. Incidentally, the above sequence of calculations involves the choice of relevant material constants as $\tilde{\kappa}''_{pr0}=6\times10^{-20}$, $\tilde{\varepsilon}''_{pr0}=1.70\times10^{-22}$, $\tilde{\kappa}'_{pr0}=10^{-12}$, $\tilde{\varepsilon}'_{pr0}=3.39\times10^{-8}$, and $\tilde{\varepsilon}_{pr0}=2.62$. We may note that the values of the second-order permittivity and chirality material constants based on the Lorentzian and Condon models turn out to be about 4 to 5 orders of magnitude larger than those that were used in the theoretical plots discussed earlier. Correspondingly, the (resonant) phase velocity for the model-based plot is also about 4 orders of magnitude higher than that for the theoretical case. Therefore, there is a consistent scaling difference between the theoretical/analytical results and those based on the practical models using typical model frequencies. This scaling difference should not be of particular concern because the analytical model simply determines the feasibility of whether a negative index is realizable or not; actual practical values and numbers would be properly determined and assessed by incorporating proper parameters in a model-based derivation.

Similarly, for the normalized group velocity, by using Eq. (29) we have

$$\tilde{v}_{g3N}(\Omega) = \frac{1}{(a+b\Omega+c\Omega^2)}, \quad (47)$$

where, $a=-1-5(\omega_0\alpha_c/\omega_c^2)+(8\omega_0\omega_p^2/\omega_c^4)$, $b=-30\omega_0\alpha_c(\omega_0/\omega_c^4)+8\omega_0(\omega_p^2/\omega_c^4)-10(\alpha_c/\omega_c^2)+(16\omega_p^2/\omega_c^4)$, $c=-45\alpha_c(\omega_0/\omega_c^4)+12(\omega_p^2/\omega_c^4)$.

The group velocity in Fig. 7 again transitions from negative to positive around the resonance. It is clear from the plot that the (positive) resonant frequency is approximately 1.20×10^{12} rad/sec. We note that the model-based material

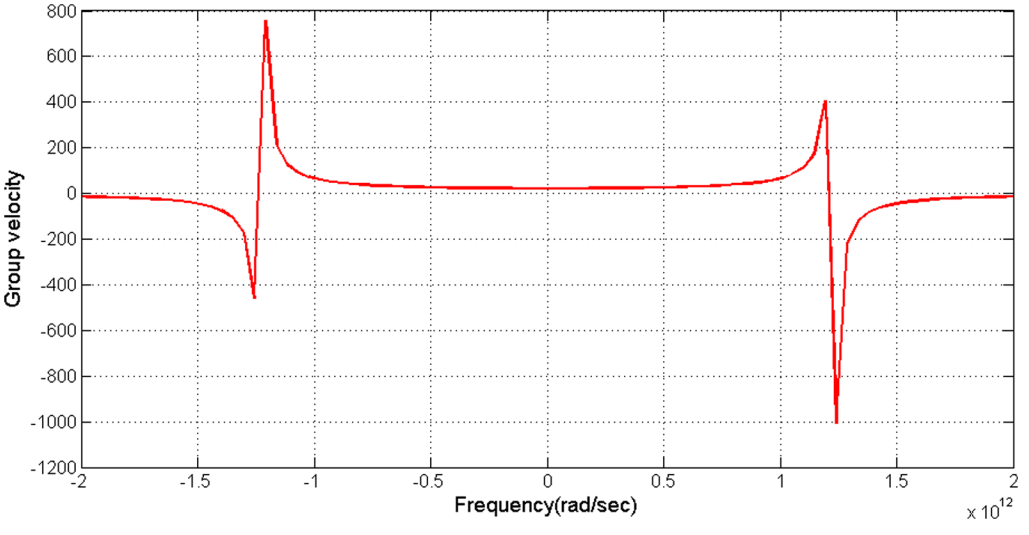

Fig. 7 The modeled group velocity under second order.

parameters for the group velocity are the same as those for the corresponding phase velocity. An important feature regarding the model-based group velocity as compared with the theoretical values obtained earlier is that for the model-based case, the resonant v_g is about 400 m/sec (and hence about 3 orders of magnitude lower than the model-based v_p), while the same for the theoretical case is dramatically lower (about 2.4×10^{-5} m/sec or less), and which is also about 6 orders of magnitude lower than the corresponding v_p. These findings are somewhat inconsistent and difficult to explain as such; however, as discussed earlier, the theoretical results are essentially feasibility studies, and the corresponding numerical values are relatively unimportant.

5.1 *Estimation of Negative Index in the Velocity Counter-Propagation Regime*

In this section, we present the graphical plots of phase and group indices under model analysis for both the first- and second-order cases. The indices are obtained by simply finding the inverse of the corresponding normalized velocities. One goal of this analysis is to ascertain if working in the second order offers any significant advantage relative to the first-order analysis. Some aspects of this were already discussed earlier in general terms; finding more quantifiable differences for the model analysis would likely enable a stronger case to be made for examining second-order material dispersion, as presented in this paper.

5.1.1 *Plot of Phase and Group Indices Under First- and Second-Order Dispersions En Route to Negative Index Material*

Noting that with $n_{p3} \triangleq 1/v_{p3N}$, and $n_{g3} \triangleq 1/v_{g3N}$, we may once again straightforwardly plot the phase and group indices for the second-order dispersive system based on the Lorentzian and Condon models. These are shown in Figs. 8(a), 8(b) and 9. Figure 8(a) depicts a zoomed version of Fig. 8(b), whereby the change of sign of the phase index is clearly visible along the frequency axis. The change of sign for the group index is evident in Fig. 9. We observe that for the given value of the parameter $\beta \triangleq (\omega_p/\omega_c) = 1.3 \times 10^{-3}$ (for the simulations here), each of the indices experiences negative values [at frequencies above 3×10^{10} rad/sec for n_{p3} as shown in Fig. 8(a)], and above 1.24×10^{12} rad/sec for n_{g3}. Hence, a negative index occurs for the model case in the frequency range 3×10^{10} rad/sec to 1.24×10^{12} rad/sec. Additionally, we note that the numerical values of both n_p and n_g under the model analysis are consistent with those discussed in the literature.[6] Thus, within the NIM region, we find that the group index is positive while the phase index is negative (hence, negative index behavior is more directly aligned with the sign of the phase index). Figures 10 and 11 show plots for the phase and group indices with first-order dispersion under the assumed models. It is seen that neither index undergoes any change of sign versus frequency. Thus, n_{p3} is positive and increases with frequency, whereas n_{g3} is negative and decreases with frequency. These characteristics, whereby n_{g3} is negative and n_{p3} is positive, are contrary to expected NIM behavior, and moreover do not show any specific NIM band. This finding agrees with previous results found in Ref 1. This last finding is significant in

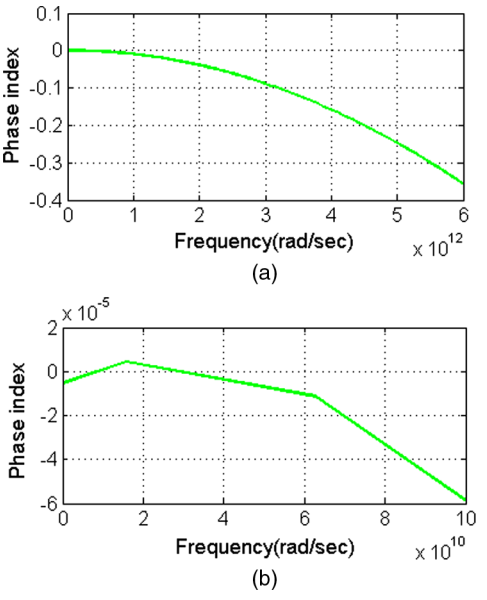

Fig. 8 Modeled phase index (a) zoom-out view; (b) zoom-in view showing positive to negative transition.

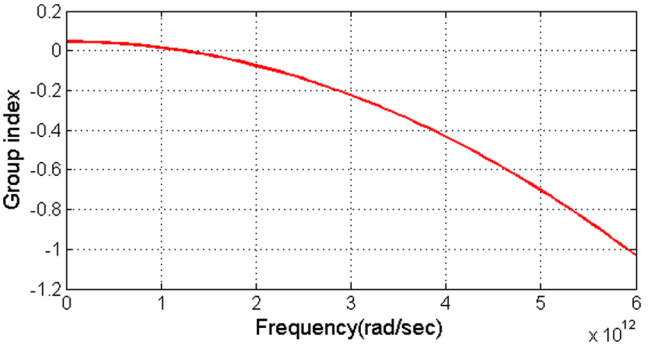

Fig. 9 Modeled group index under second-order dispersion.

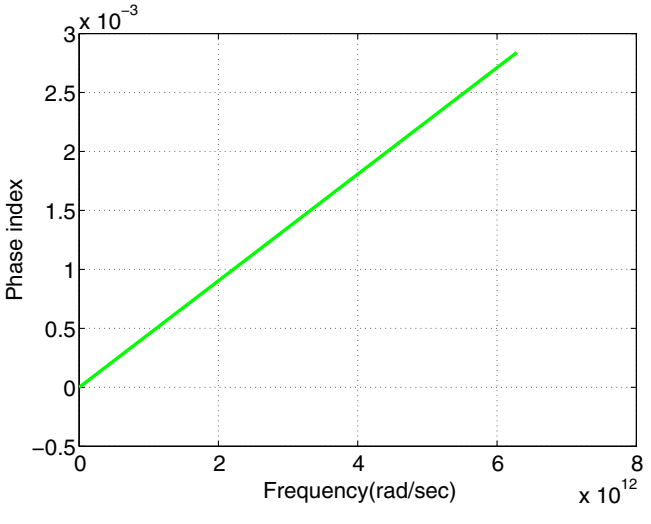

Fig. 10 Modeled phase index under first order.

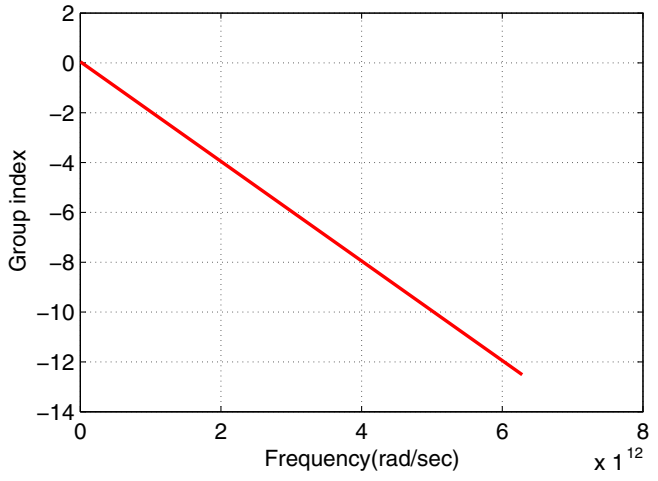

Fig. 11 Modeled group index under first order.

that under material dispersion models, NIM is achievable based on this analysis only under second-order dispersion.

6 Conclusion

Starting from the phasor approach and slowly varying the envelope approximation combined with Maxwell's equations and the constitutive relations in a reciprocal chiral material, expressions for electromagnetic phase and group velocities have been derived assuming second-order material dispersion. It is seen that in the presence of chirality, the propagating EM field is always circularly polarized independent of dispersion. As was the case for first-order dispersion, it is found that once again a negative index may also be realized under second-order conditions. It is important to note that the NIM behavior as seen here for both first- and second-order cases occurs under the parametric analysis with arbitrarily chosen numerical values of dispersive parameters. It is demonstrated that there are measurable ranges of frequency where the phase and group velocities are in opposition for identical material properties, leading to the emergence of NIM over a specific frequency band. Phase and group velocities based on the application of Lorentzian and Condon models are also derived and plotted, and thereby compared case by case for compatible choices of model-based material parameters. We note that the sideband resonances for both v_p and v_g range in the neighborhoods of 100 Mrad/sec to 10 Grad/sec under parametric analysis. Actual carrier frequencies will, of course, be much higher, as described in the text. Also, the derived velocity resonances for the analytical cases appear to be impractical; however, the numerical values are relatively unimportant for the theoretical (i.e., parametric) analyses as long as the possible emergence of a negative index is established as feasible. Phase and group indices for the model-based analyses under the second-order have also been derived and plotted, and indicate regions of negative excursions. It is found that NIM behavior using the model-based analyses occurs only under second-order dispersion. When the indices are examined under first order, we find that for the chosen practical parameter values, NIM does not occur. Moreover, the physical range of index values found under model-based analyses is compatible with that seen in the literature. The absence of NIM under first-order model-based analyses demonstrates a significant difference from the corresponding second-order result, thereby highlighting the importance of second-order analysis as pursued in this paper.

Acknowledgments

The authors (MRC and TA) would like to thank the ECE Department for providing travel support toward presentation of this work. TA would also like to acknowledge the financial support provided by the Libyan Government higher education program for this research.

References

1. P. P. Banerjee and M. R. Chatterjee, "Negative index in the presence of chirality and material dispersion," *J. Opt. Soc. Am. B* **26**, 194–202 (2009).
2. J. B. Pendry, "Negative refraction," *Contemp. Phys.* **45**, 191–202 (2004).
3. V. G. Veselago et al., "Negative refractive index materials," *Comput. Theor. Nanosci.* **3**, 1–30 (2006).
4. A. Lakhtakia, V. K. Varadan, and V. V. Varadan, *Time-Harmonic Electromagnetic Fields in Chiral Media*, Springer-Verlag, New York (1989).
5. S. Zhang et al., "Negative refractive index in chiral metamaterials," *Phys. Rev. Lett.* **3**, 023901 (2010).
6. M. R. Chatterjee and T. A. Algadey, "Investigation of negative index in dispersive chiral materials via contra-propagating velocities under second-order dispersion GVD," *Proc. SPIE* **8837**, 88370W (2013).
7. R. A. Shelby, D. R. Smith, and S. Shultz, "Experimental verification of a negative index of refraction," *Science* **292**, 77–79 (2002).
8. W. J. Padilla, D. N. Basov, and D. R. Smith, "Negative refractive index metamaterials," *Mater. Today* **9**, 7–8 (2006).
9. V. G. Veselago, "The electrodynamics of substances with simultaneously negative values of ε and μ," *Sov. Phys. USP* **10**(4), 509–514 (1968).
10. P. M. Valanju, R. M. Walser, and A. P. Valanju, "Wave refraction in negative-index media: always positive and very inhomogenous," *Am. Phys. Soc.* **88**, 18740–4 (2002).
11. Z. G. Dong, S. N. Zhu, and H. LIU, "Numerical simulations of negative-index refraction in wedge-shaped metamaterials," *Am. Phys. Soc.* **72**, 016607 (2005).
12. D. R. Smith et al., "Composite medium with simultaneously negative permeability and permittivity," *Phys. Rev. Lett.* **84**(18), 4184–4187 (2000).
13. J. Valentine et al., "Three- dimensional optical metamaterial with a negative refractive index," *Nature* **455**, 376–379 (2008).
14. H. Chen and M. Chen, "Flipping photons backward: reversed Cherenkov radiation," *Mat. Today* **14**(1–2), 34–41 (2011).
15. V. M. Shalaev, "Optical negative-index metamaterials," *Nat. Photonics* **1**, 41–48 (2007).
16. J. B. Pendry and D. R. Smith, "Reversing light with negative refraction," *Phys. Today* **57**, 37–43 (2004).
17. P. Yeh, *Optical Waves in Layered Media*, Springer-Verlag, Wiley, New York (1988).
18. P. P. Banerjee and G. Nehmetallah, "Linear and nonlinear propagation in negative index materials," *Opt. Soc. Am.* **23**, 2348–2358 (2006).
19. P. G. Zablocky and N. Engheta, "Transients in chiral media with single-resonance dispersion," *Opt. Soc. Am.* **10**, 740–751 (1993).

Monish R. Chatterjee has been a professor of electrical and computer engineering (ECE) at the University of Dayton since 2002. He has authored over 60 papers in archival journals and conference proceedings, several book chapters, three literary books, numerous literary essays, and presented over 100 papers at international conferences. He is a senior member of the IEEE and the OSA, and a member of SPIE and Sigma Xi.

Tarig A. Algadey received his BSEE degree in communication engineering from the College of Industrial Technology, Misurata, Libya, in 2001, and his MSEE degree from the Libya Academy of Graduate Studies, Tripoli, Libya, in 2008. Currently, he is completing his research for his PhD degree at the University of Dayton, Dayton, Ohio. His research interests include negative index in complex media, metamaterials, electromagnetics, and digital communications.